# A NUMERICAL STUDY OF LINEARIZED KELLER-SEGEL OPERATOR IN SELF-SIMILAR VARIABLES

JUAN F. CAMPOS, JEAN DOLBEAULT

Abstract. This report is devoted to a numerical study of the Keller-Segel model in self-similar variables. We first parametrize the set of solutions in terms of the mass parameter $M \in (0, 8\pi)$ and consider the asymptotic regimes for $M$ small or $M$ close to $8\pi$. Next we introduce the linearized operator and study its spectrum using various shooting methods: we determine its kernel, the spectrum among radial functions and use a decomposition into spherical harmonics to study the other eigenvalues. As a result, we numerically observe that the spectral gap of the linearized operator is independent of $M$ and equal to 1, which is compatible with known results in the limiting regime corresponding to $M \to 0_+$, and with recent theoretical results obtained by the authors. We also compute other eigenvalues, which allows to state several claims on various refined asymptotic expansions of the solutions in the large time regime.

In its simplest version, the parabolic-elliptic Keller-Segel model (also known as the Patlak-Keller-Segel model, see [13, 10])

$$\text{(1)} \qquad \begin{cases} \frac{\partial u}{\partial t} = \Delta u - \nabla \cdot (u \, \nabla v) & x \in \mathbb{R}^2 \,, \quad t > 0 \\ v = -\frac{1}{2\pi} \log |\cdot| * u & x \in \mathbb{R}^2 \,, \quad t > 0 \\ u(0, x) = n_0 \geq 0 & x \in \mathbb{R}^2 \end{cases}$$

describes the motion of unicellular amoebae, like *dictyostelium discoideum,* which move freely and diffuse. Here $u$ denotes their spatial density and it makes sense to consider them in a two-dimensional setting like the one of a Petri dish. Under certain circumstances, they emit a *chemo-attractant* and eventually start to aggregate by moving in the direction of the largest concentration of the chemo-attractant. This is modeled in the above equations by the drift term $\nabla \cdot (u \, \nabla v)$. The life cycle of *dictyostelium discoideum* has attracted lots of attention in the community of biologists. Trying to understand the competition between the diffusion and the drift is a key issue in the aggregation process, which has also motivated quite a few studies among mathematicians interested in applications of PDEs to biology. See [14] for a recent overview on the topic.

*Date*: May 30, 2012.

*Email addresses:* campos@ceremade.dauphine.fr and juanfcampos@gmail.com, dolbeaul@ceremade.dauphine.fr.

An easy computation (see [14, pages 122–124] and [11]) shows that solutions (with second moment initially finite) blow-up in finite time if the total mass is large enough (larger than $8\pi$ with our conventions), that is they describe an aggregate, while, for solutions with smaller masses, the diffusion dominates the large time asymptotics.

More precisely, it has been shown in [9, 7, 4] that, for initial data $n_0 \in L^1_+\big(\mathbb{R}^2\,,(1+|x|^2)\,dx\big)$ such that $n_0\,|\log n_0| \in L^1(\mathbb{R}^2)$ and $M := \int_{\mathbb{R}^2} n_0\,dx < 8\pi$, there exists a solution $u$, in the sense of distributions, that is global in time and such that $M = \int_{\mathbb{R}^2} u(x,t)\,dx$ is preserved along the evolution. There is no non-trivial stationary solution to (1) and any solution converges to zero locally as time gets large. In order to study the asymptotic behavior of $u$, it is therefore convenient to work in self-similar variables. In the space and time scales given respectively by $R(t) := \sqrt{1+2t}$ and $\tau(t) := \log R(t)$, we define the rescaled functions $n$ and $c$ by

$$u(x,t) := R^{-2}\,n\left(R^{-1}(t)\,x,\tau(t)\right) \quad \text{and} \quad v(x,t) := c\left(R^{-1}(t)\,x,\tau(t)\right)\ .$$

This time-dependent rescaling is the one of the heat equation. Since the nonlinear term is invariant under this rescaling, it is also present in the rescaled system without time-dependent coefficient. This system can be written as

$$\left\{\begin{array}{ll} \frac{\partial n}{\partial t} = \Delta n + \nabla\cdot(n\,x) - \nabla\cdot(n\,\nabla c) & x\in\mathbb{R}^2\,,\quad t>0\\ c = -\frac{1}{2\pi}\log|\cdot| * n & x\in\mathbb{R}^2\,,\quad t>0\\ n(0,x) = n_0 \ge 0 & x\in\mathbb{R}^2 \end{array}\right. \tag{2}$$

and it has been shown in [4] that $n$ and $\nabla c$ converge as $t\to\infty$, respectively in $L^1(\mathbb{R}^2)$ and $L^2(\mathbb{R}^2)$ to a unique stationary solution given by smooth and radially symmetric functions.

In this report, we are interested in estimating the rate of convergence towards the stationary solution in self-similar variables. After undoing the change of variables, this gives the rate of convergence towards the asymptotic profile for the solutions of (1). Existence of a stationary solution to (2) has been established in [1] by ODE techniques, and in [12] by PDE methods. The uniqueness has been shown in [2]. In [3], it has been proved that if $M$ is less than some mass $M_* \in (0,8\pi)$, then convergence holds at an exponential rate, which is essentially governed by the linearization of System (2) around the stationary solution. However, the estimate of the value of $M_*$ was found to be significantly smaller than $8\pi$. In the radially symmetric setting, V. Calvez and J.A. Carrillo have found in [5] that the rate measured with respect to Wasserstein's distance does not depend on the mass, in the whole range $(0,8\pi)$. Refined estimates have recently been established in [6], in which the functional setting for the linear operator has also been properly characterized. We will recover all these results numerically and give more detailed estimates on the asymptotic behavior of the solutions.

Consider the unique stationary solution to (2), which is characterized as the solution to

$$-\Delta c = n = M\,\frac{e^{-\frac12\,|x|^2+c}}{\int_{\mathbb{R}^2} e^{-\frac12\,|x|^2+c}\,dx}\,,\quad x\in\mathbb{R}^2 \tag{3}$$

for any given mass $M\in(0,8\pi)$. The bifurcation diagram of the solutions in terms of the parameter $M$ will be considered in Section 1.

Next, consider $f$ and $g$ such that $n\,(1+f(x,t))$ and $c(x)\,(1+g(x,t))$ is a solution to (2). Then $(f,g)$ solves the nonlinear problem

$$\begin{cases} \frac{\partial f}{\partial t}-\mathcal{L}\,f=-\frac1n\,\nabla\cdot[f\,n\,(\nabla(g\,c))] & x\in\mathbb{R}^2\,,\quad t>0\\ -\Delta(c\,g)=f\,n & x\in\mathbb{R}^2\,,\quad t>0 \end{cases}$$

where $\mathcal{L}$ is the linear operator defined by

$$\mathcal{L}\,f=\frac1n\,\nabla\cdot[n\,\nabla(f-c\,g)]$$

and we know that $(f\,n,\nabla(g\,c))(t,\cdot)$ has to evolve in $L^1(\mathbb{R}^2)\times L^2(\mathbb{R}^2)$, and asymptotically vanish as $t\to\infty$. To investigate the large time behavior, it is convenient to normalize the solution differently. What we actually want to investigate is the case where solutions of (2) can be written as

$$n(x)\,(1+\varepsilon\,f(x,t))\quad\text{and}\quad c(x)\,(1+\varepsilon\,g(x,t))$$

in the asymptotic regime corresponding to $\varepsilon\to0_+$. Formally, it is then clear that, at order $\varepsilon$, the behavior of the solution is given by $\frac{\partial f}{\partial t}=\mathcal{L}\,f$. The kernel of $\mathcal{L}$ has been identified in [6]. It has also been shown that $\mathcal{L}$ has pure discrete spectrum and that 1 and 2 are eigenvalues. In this report, our goal is to identify the lowest eigenvalues and recover that the spectral gap is actually equal to 1, whatever the mass is in the range $M_*\in(0,8\pi)$. We will also establish the numerical value of other eigenvalues of $\mathcal{L}$ at the bottom of its spectrum in Section 3, and draw some consequences in the last section of this report: improved rates of convergence for centered initial data and faster decay rates for best matching self-similar solutions.

## 1. Bifurcation diagram and qualitative properties of the branch of solutions corresponding to $M\in(0,8\pi)$

We can numerically solve (3) among radial solutions as follows. Let

$$\phi(r)=b+c(x)$$

for some $b\in\mathbb{R}$, $r=|x|$, for any $x\in\mathbb{R}^2$, such that

$$M\,\frac{e^{-b}}{\int_{\mathbb{R}^2} e^{-\frac12\,|x|^2+c}\,dx}=1\quad\Longleftrightarrow\quad b=\log M-\log\left(\int_{\mathbb{R}^2} e^{-\frac12\,|x|^2+c}\,dx\right).$$

Then the function $r\mapsto\phi(r)$ solves

$$-\phi''-\frac1r\,\phi'=e^{-\frac12\,r^2+\phi}\,,\quad r>0$$

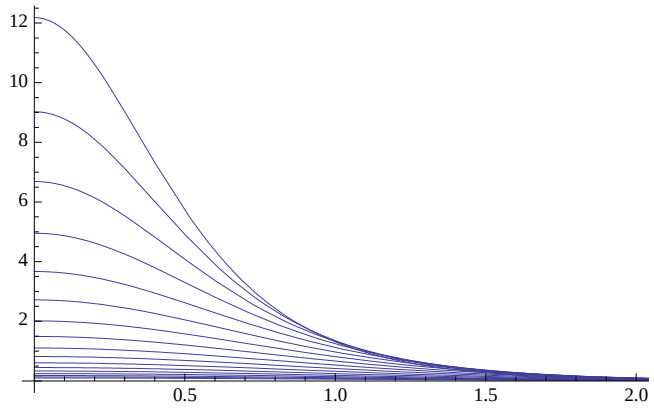


FIGURE 1. *The density $n_a$ as a function of $r = |x|$ for $a = -2.3, -1.9, \ldots -0.2, 0.1, 0.4, 0.7 \ldots 2.5$.*

with initial conditions $\phi(0) = a$, $\phi'(0) = 0$. To emphasize the dependence in $a \in \mathbb{R}$, we will denote the solution by $\phi_a$. Since

$$1 = M\,\frac{1}{\int_{\mathbb{R}^2} e^{-\frac{1}{2}\,|x|^2+b+c}\,dx} = \frac{M}{2\pi\int_0^\infty r\,e^{-\frac{1}{2}\,r^2+\phi}\,dr}\,,$$

all radial solutions of (3) can therefore be parametrized by $a \in \mathbb{R}$, using $M = M(a)$ with

$$M(a) := 2\pi\int_0^\infty e^{-\frac{1}{2}\,r^2+\phi_a}\,dr\,.$$

The density

$$n_a(x) := M(a)\,\frac{e^{-\frac{1}{2}\,|x|^2+c_a}}{\int_{\mathbb{R}^2} e^{-\frac{1}{2}\,|x|^2+c_a}\,dx}\,,\quad x \in \mathbb{R}^2$$

can be directly computed as

$$n_a(x) = M(a)\,\frac{e^{-\frac{1}{2}\,r^2+\phi_a(r)}}{2\pi\int_0^\infty r\,e^{-\frac{1}{2}\,r^2+\phi_a}\,dr} = e^{-\frac{1}{2}\,r^2+\phi_a(r)}$$

with $r = |x|$ (see Fig. 1).

Moreover it is clear that $c$ in (3) is determined only up to the addition of a constant. This constant can be fixed by assuming that

$$\lim_{|x|\to\infty}\left(c(x) + \frac{M}{2\pi}\,\log|x|\right) = 0\,,$$

and we will denote by $c_a$ the corresponding solution. Hence, with

$$b(a) := \lim_{r\to\infty}\left(\phi_a(r) + \frac{M(a)}{2\pi}\,\log r\right)$$

we finally recover that

$$c_a(x) = \phi_a(|x|) - b(a)$$

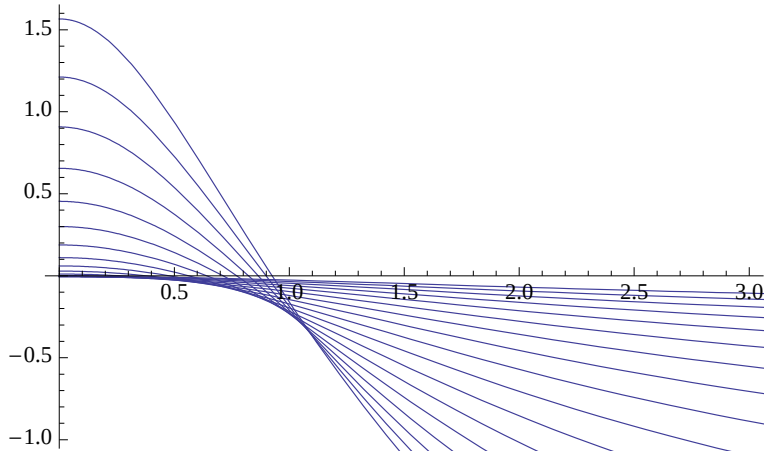


FIGURE 2. *The function $c_a$ as a function of $r = |x|$ for $a = -2.3, -1.9, \ldots\ 2.5$.*

(see Fig. 2).

The above considerations allow to parametrize by $a$ the bifurcation diagram of the solutions of (3) in $L^\infty(\mathbb{R}^2)$ in terms of the mass $M$: see Figs. 3 and 4.

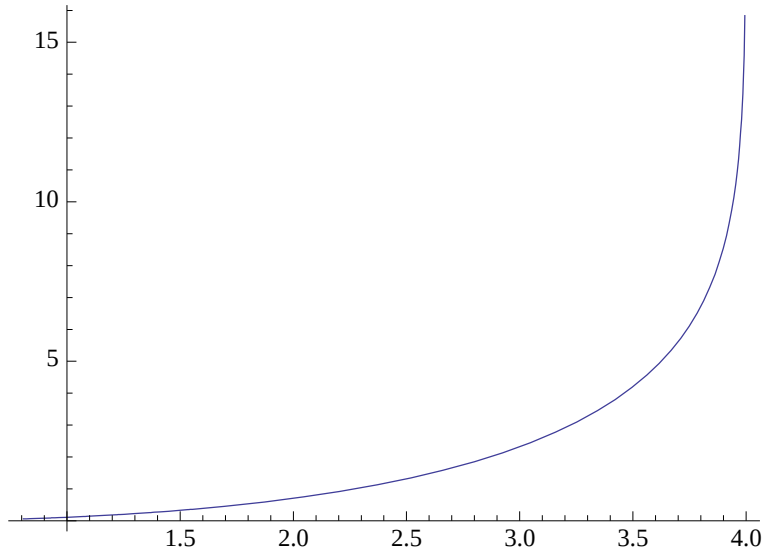


FIGURE 3. *The bifurcation diagram associated to solutions of (3) can be parametrized by $a \mapsto (\frac{1}{2\pi} M(a), \|c_a\|_{L^\infty(\mathbb{R}^2)})$. Here $\|c_a\|_{L^\infty(\mathbb{R}^2)} = c_a(0) = a - b(a)$. Such a diagram is qualitatively very similar to the one of the Keller-Segel system in a ball with no flux boundary conditions.*

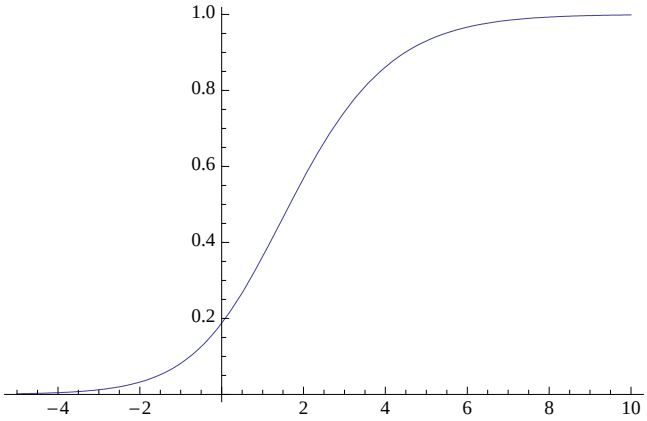


FIGURE 4. *The mass can be computed as*

$$M(a) = 2\pi \int_0^\infty n_a(r)\, r\, dr \ .$$

*Plot of* $a \mapsto \frac{1}{8\pi}\, M(a)$.

## 2. Asymptotic regimes

Before studying the eigenvalue problem associated to $\mathcal{L}$, it makes sense to investigate the limiting behaviors of the solutions of (3) as $a \to +\infty$ and $a \to 0$, in order to check the accuracy of our numerical approach. The regime $a \to +\infty$ is by itself interesting. Roughly speaking, concentration, which is numerically observed as the mass $M$ approaches $8\pi$, suggests that for $M = 8\pi$ the limiting problem is governed by the stationary solutions of (1). This is indeed what occurs and is confirmed by a simple asymptotic expansion.

2.1. **The large, positive $a$ regime.** It can be numerically observed in Fig. 3 that

$$\lim_{a\to+\infty} M(a) = 8\pi \ .$$

With $\lambda(a) = 2\sqrt{2}\, e^{-a/2}$, we moreover observe that $\lambda(a)^2\, n_a(\lambda(a)\, x)$ converges as $a \to +\infty$ to

$$n_\star(x) := \frac{8}{(1+|x|^2)^2} \ , \quad x \in \mathbb{R}^2$$

which is the well known solution to the unscaled Keller-Segel model with mass $8\pi = \int_{\mathbb{R}^2} n_\star\, dx$. See Fig. 5.

The following asymptotics are not very difficult to recover heuristically. Let

$$c_\star(x) := -2\log(1+|x|^2) \ , \quad x \in \mathbb{R}^2$$

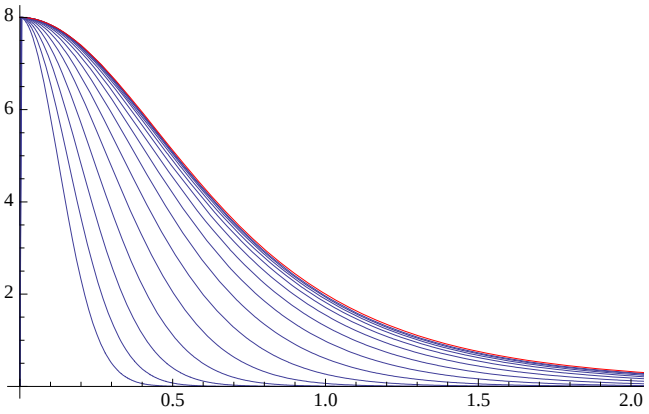


FIGURE 5. *The $a \to +\infty$ case. As a function of $r = |x|$, $\lambda(a)^2\, n_a(\lambda(a)\, x)$ is plotted in blue for $a = -2,\ -1.5,\ldots\ 5$, while the limiting profile $r \mapsto n_\star(r)$ is shown in red.*

and observe that $c_\star$ solves

$$-\Delta c_\star = 8\pi\, \frac{e^{c_\star}}{\int_{\mathbb{R}^2} e^{c_\star}\, dx} = n_\star$$

with $8\pi\, e^{c_\star} / \int_{\mathbb{R}^2} e^{c_\star}\, dx = n_\star$. Actually all radial solutions of the above equation are of the form $x \mapsto (\lambda^2\, n_\star(\lambda\, x), c_\star(\lambda\, x) + \mu)$ for any $\lambda > 0$ and $\mu \in \mathbb{R}$. Now, for our special choice of $c_\star$, we have $\int_{\mathbb{R}^2} e^{c_\star}\, dx = \pi$, and hence $c_\star$ is the unique solution to

$$-\Delta c_\star = 8\, e^{c_\star}$$

such that $c_\star(0) = 0$. Let $\psi_a(r) := \phi_a(\lambda\, r) - a$ and observe that

$$-\psi_a'' - \frac{1}{r}\, \psi_a' = e^{\psi_a + a + 2\log\lambda + \frac{\lambda^2}{2}\, r^2} = 8\, e^{\psi_a + \frac{\lambda^2}{2}\, r^2}$$

if $\lambda = \lambda(a) = 2\,\sqrt{2}\, e^{-a/2}$. Hence, since $\psi_a(0) = 0$ and $\lim_{a\to\infty} \lambda(a) = 0$, it is clear that $\psi_a$ converges to $c_\star$. This justifies the fact that $\lambda(a)^2\, n_a(\lambda(a)\, \cdot)$ converges to $n_\star$ as $a \to +\infty$.

2.2. **The large, negative $a$ regime.** When $a \to -\infty$, it is elementary to observe that $a - \phi_a(r) \sim e^a\, \psi(r)$ where $\psi$ solves

$$-\psi'' - \frac{1}{r}\, \psi' = e^{-\frac{1}{2}\, r^2}$$

with $\psi(0) = \psi'(0) = 0$. Integrating this equation, we find that

$$2\, \psi(r) := \int_0^{r^2/2} \left(1 - e^{-s}\right)\, \frac{ds}{s} = \gamma + \Gamma(0, \tfrac{1}{2}\, r^2) - \log 2 + 2\, \log r\ .$$

Here $\Gamma(x, y) = \int_y^{+\infty} t^{x-1}\, e^{-t}\, dt$ is the *Incomplete Gamma Function* and $\gamma \approx 0.577216$ is *Euler's constant.* See Fig. 6.

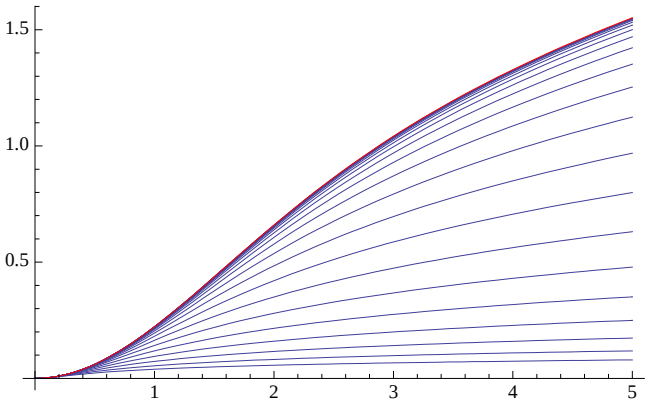


FIGURE 6. *The $a \to -\infty$ case. The function $e^{-a}\,(a-\phi_a)$ as a function of $r=|x|$ for $a=-5,\,-4.5,\ldots\,5$ and the limiting profile $r\mapsto\psi(r)$ (in red).*

## 3. Linearization and spectral gap

Consider the linearized Keller-Segel operator $\mathcal{L}$ introduced at the beginning of this report. Since the function $n_a$ is involved in the linearization, to emphasize the dependence in the parameter $a$, we shall use the notation $\mathcal{L}_a$. Recall that this operator is defined by

$$\mathcal{L}_a\,f:=\frac{1}{n_a}\nabla\cdot\left[n_a\,\nabla(f-\varphi_f)\right]\ ,\quad x\in\mathbb{R}^2$$

where

$$-\Delta\,\varphi_f=n_a\,f\ .$$

3.1. **Kernel of $\mathcal{L}_a$.** A derivation of $\phi_a$ with respect to $a$ provides a solution to $\mathcal{L}_a\,f=0$, $f(0)=1$, $f'(0)=0$. By the Cauchy-Lipschitz theorem (and an appropriate analysis at $r=0$), this solution is unique. See [6] for more details. Hence we have found a solution $f_a$ of

$$-f_a''-\frac{1}{r}\,f_a'=e^{-\frac{1}{2}\,r^2+\phi_{f_a}}\,f_a\ ,\quad r>0$$

with initial conditions $f_a(0)=1$ and $f_a'(0)=0$, which generates $\mathrm{Ker}(\mathcal{L}_a)$. See Figs. 7 and 8 for some plots of the solution for various values of $a$.

3.2. **Non-zero eigenvalues of $\mathcal{L}_a$.** According to [6], $\mathcal{L}_a$ has no continuous spectrum. All non-zero eigenvalues of $-\mathcal{L}_a$ are positive and hence there is a positive spectral gap that can be fully determined using a decomposition in spherical harmonics: for a given $a\in\mathbb{R}$, the spectrum is obtained by solving the radial eigenvalue problems

$$-\mathcal{L}_a^{(k)}\,f_{k,\ell}=\lambda_{k,\ell}\,f_{k,\ell}\ ,\quad \ell\in\mathbb{N}$$

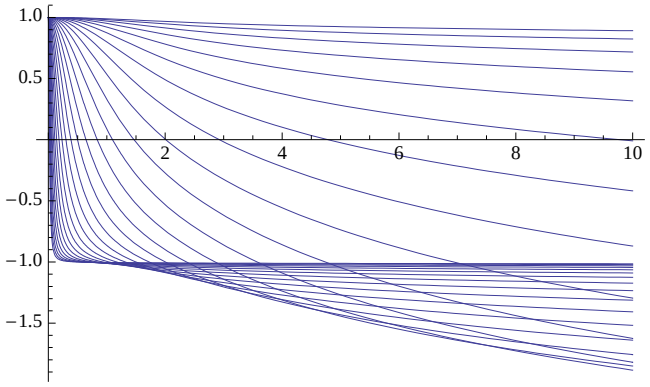


FIGURE 7. *The function $f_a$ as a function of $r = |x|$ for $a = -3, -2, \ldots 10$.*

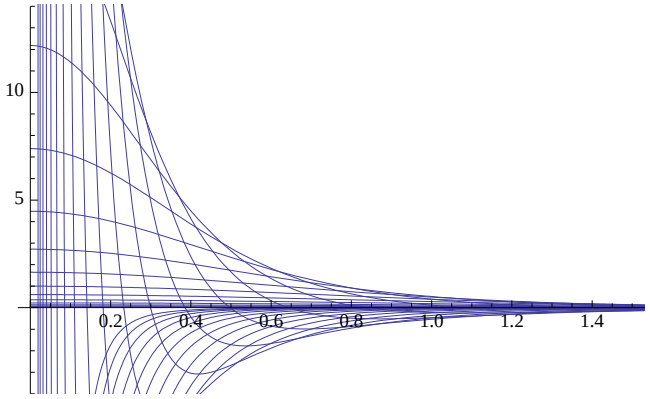


FIGURE 8. *The density $f_a\, n_a$ as a function of $r = |x|$ for $a = -3, -2, \ldots 10$.*

where, for any $k \in \mathbb{N}$,

$$-\mathcal{L}_a^{(k)} f = -f'' - \frac{1}{r} f' + \frac{k^2}{r^2} f + (r - c_a') (f' - \psi') - n_a f$$

and, with previous notations, $\psi = c_a\, g$ is obtained as the solution to

$$-\psi'' - \frac{1}{r} \psi' + \frac{k^2}{r^2} \psi = n_a f \ .$$

Here we draw the attention of the reader about the numbering of the eigenvalues, which differs from the one adopted in [6].

3.3. **Spectrum of $\mathcal{L}_a$ restricted to radial functions.** To determine the spectrum of $\mathcal{L}_a^{(0)}$, we can use a simple shooting method that goes as follows. Owing to the fact that if $\lambda$ is an eigenvalue, then $\lim_{r\to\infty} f(r) = 0$, we solve the equation

$$\mathcal{L}_a^{(0)} f + \lambda f = 0$$

with initial conditions $f(0) = 1$ and $f'(0) = 0$. We numerically recover that $\lambda = 0$ is an eigenvalue and find that the lowest non-zero eigenvalue of $-\mathcal{L}_a^{(0)}$ is exactly 2. See Figs. 9–13. This is consistent with the results of [5].

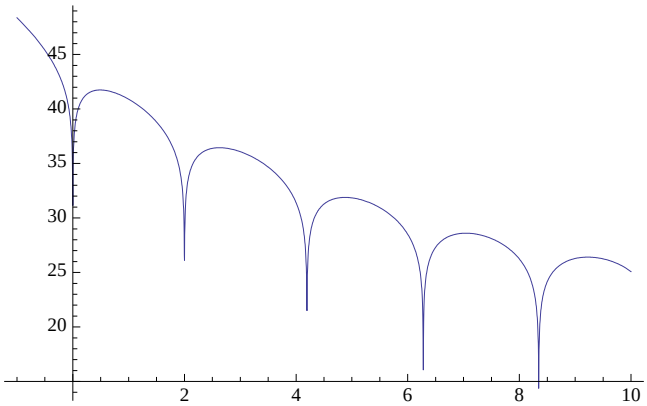


FIGURE 9. *Plot of* $\lambda \mapsto \log\left(1 + f(\lambda, R)^2\right)$ *with* $R = 7$, $a = 1$, *where* $r \mapsto f(\lambda, r)$ *is the solution to* $\mathcal{L}_a^{(0)} f + \lambda f = 0$ *such that* $f(0) = 1$ *and* $f'(0) = 0$. *Each local minimum corresponds to an eigenvalue in the limit* $R \to \infty$. *First minima (from the left) are located exactly at* $\lambda = 0$ *and* $\lambda = 2$.

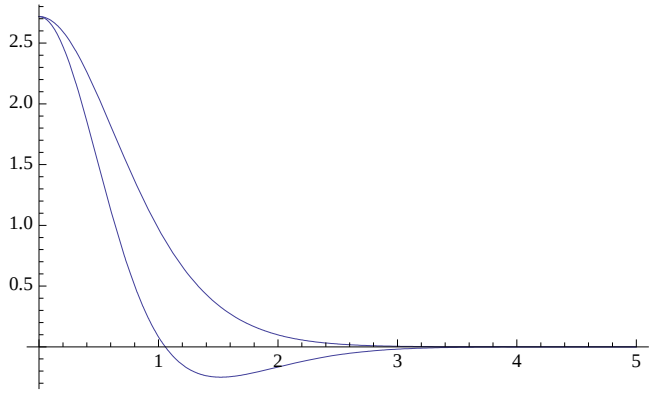


FIGURE 10. *Plot of* $r \mapsto n_a(r)$ *and* $r \mapsto n_a(r)\, f(r)$ *for* $a = 1$, $\lambda = 2$. *The eigenfunction* $f$ *changes sign once. The total mass for* $a = 1$ *is* $M(a) = 2\pi \int_0^\infty n_a(r)\, r\, dr \approx 9.10875$.

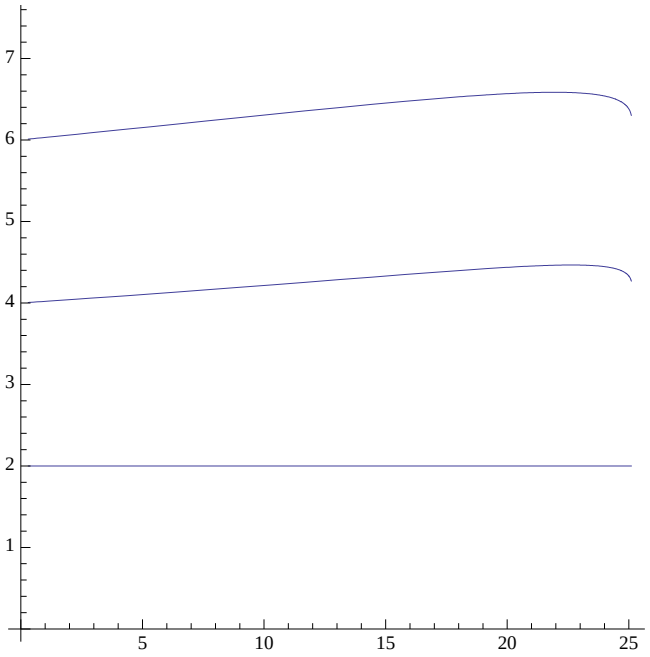


FIGURE 11. *Lowest eigenvalues in the spectrum in* $\mathcal{L}_a^{(0)}$*, as a function of* $M = M(a)$*.*

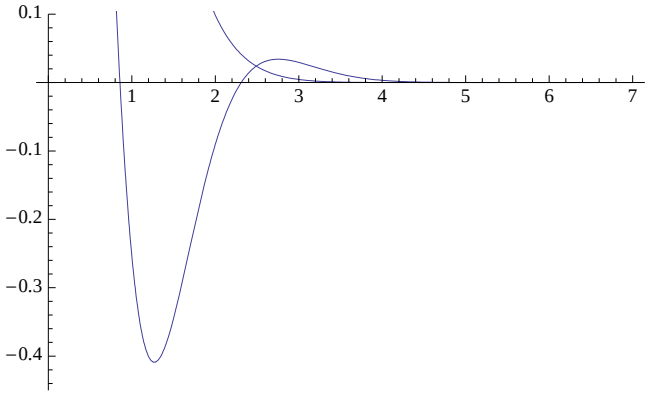


FIGURE 12. *Detail of the plots of* $r \mapsto n_a(r)$ *and* $r \mapsto n_a(r)\, f(r)$ *for* $a = 1$*,* $\lambda \approx 4.1944$*. The eigenfunction* $f$ *changes sign twice.*

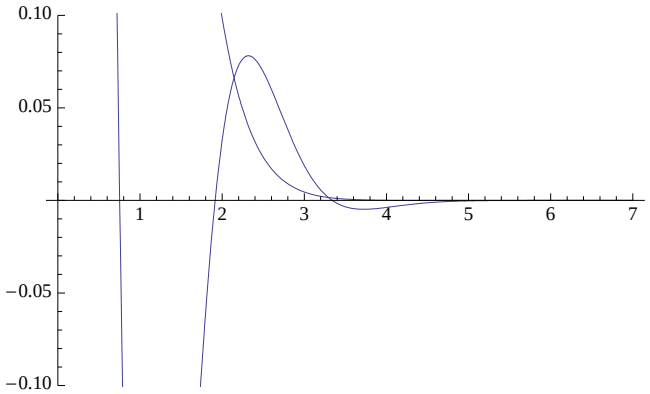


FIGURE 13. *Detail of the plots of* $r \mapsto n_a(r)$ *and* $r \mapsto n_a(r)\, f(r)$ *for* $a = 1$, $\lambda \approx 6.27881$. *The eigenfunction* $f$ *changes sign three times.*

3.4. **Spectrum of $\mathcal{L}_a^{(1)}$: the $k = 1$ component of the spectrum.** By construction, we know that the spectrum $\mathrm{sp}(\mathcal{L}_a)$ of $\mathcal{L}_a$ can be decomposed using the spherical harmonics decomposition as

$$\mathrm{sp}(\mathcal{L}_a) = \bigcup_{k\in\mathbb{N}} \mathrm{sp}\big(\mathcal{L}_a^{(k)}\big)$$

where

$$\mathrm{sp}\big(\mathcal{L}_a^{(k)}\big) = (\lambda_{k,\ell})_{\ell\in\mathbb{N}}$$

for any $k \in \mathbb{N}$. Recall that $\{\lambda_{0,0}\}$ corresponds to the kernel of $\mathcal{L}_a$:

$$\lambda_{0,0} = 0\ .$$

Moreover, we know that these spectra are ordered, in the sense that

$$\lambda_{k_1,\ell} \le \lambda_{k_2,\ell} \quad \text{if} \quad k_1 \le k_2\ .$$

As a consequence, to determine the spectral gap, we only need to find the minimum of $\lambda_{0,1}$ and $\lambda_{1,0}$.

Numerically, we have observed that $\lambda_{0,1} = 2$ is an eigenvalue. This mode associated is to dilations. The mode associated to translations is in the component $k = 1$ and corresponds to an eigenvalue $\lambda_{1,\ell} = 1$, for some $\ell$ to be determined. See [6] for the justification of the role of dilations and translations, and Section 4 for more detailed comments. Let us check numerically that $\ell = 0$ (*i.e.* that there is no other mode in the component $k = 1$ corresponding to an eigenvalue in $(0, 1)$), so that the spectral gap is

$$\lambda_{1,0} - \lambda_{0,0} = 1$$

and that this holds true for any value of $a \in \mathbb{R}$.

For this purpose, we determine $(\lambda_{k,\ell})_{\ell\in\mathbb{N}}$ by solving the system of ODEs

$$-f'' - \frac{1}{r}\,f' + \frac{k^2}{r^2}\,f + (r - c_a')\,(f' - \psi') - n_a\,f = \lambda\,f\ ,$$
$$-\psi'' - \frac{1}{r}\,\psi' + \frac{k^2}{r^2}\,\psi = n_a\,f\ .$$

Boundary conditions have to be determined appropriately. Let us focus on the case $k = 1$. We may fix $f(0) = 0$, $f'(0) = 1$ and $\psi(0) = 0$ without restriction. However, $p = -\psi'(0)$ has to be determined, and this cannot be done by a simple Taylor expansion around $r = 0_+$, as can be checked to the price of a painful computation, that we shall omit here. A numerical scheme has therefore to be invoked.

Before doing so, let us make an ansatz, which turns out to be very convenient. For the special choice of $\psi'(0) = -\frac{e^a}{e^a+2}$, we can plot $\lambda \mapsto \log\left(1 + f(\lambda, R)^2\right)$ as for the case $k = 0$. See Fig. 14. An explanation for this ansatz will be given below. The lowest eigenvalue found in the framework of this ansatz has the value 1 and corresponds to

$$f(r) = v_a'(r) - r\ , \quad \psi(r) = c_a'(r) \quad \forall\ r > 0\ .$$

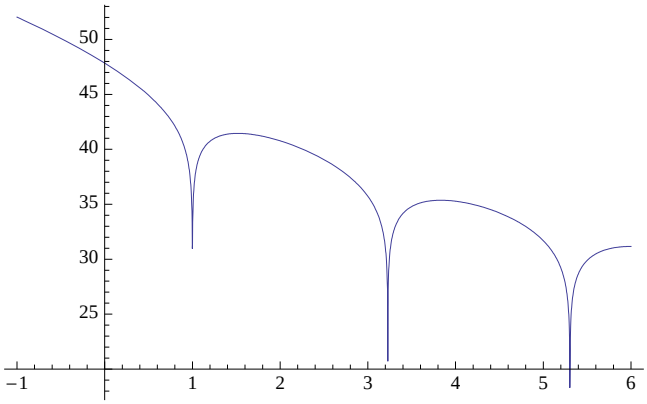


FIGURE 14. *Plot of* $\lambda \mapsto \log\left(1 + f(\lambda, R)^2\right)$ *with* $R = 7$, $a = 1$, *where* $r \mapsto f(\lambda, r)$ *is the solution to* $\mathcal{L}_a^{(1)} f + \lambda\, f = 0$ *such that* $f(0) = 1$, $f'(0) = 0$, $\psi(0) = 0$ *and* $\psi'(0) = -\frac{e^a}{e^a+2}$. *In the limit* $R \to \infty$, *the first minimum (from the left) is located exactly at* $\lambda = 1$. *However, because of the ansatz, we have no guarantee that there is no other eigenvalues, or even that the other minima are actually eigenvalues. With* $R = 7$, *the second minimum (from the left) is achieved for* $\lambda \approx 3.22762$. *See Fig. 15.*

Now let us come back to the general case. For a given $a$ and $\lambda$, we can consider the function which associates to a given $p > 0$ the value of $h(a, \lambda, p, R) := \int_0^R (|f'|^2 + |f|^2)\, n_a\, r\, dr$, for $R$ large enough. See Fig. 16.

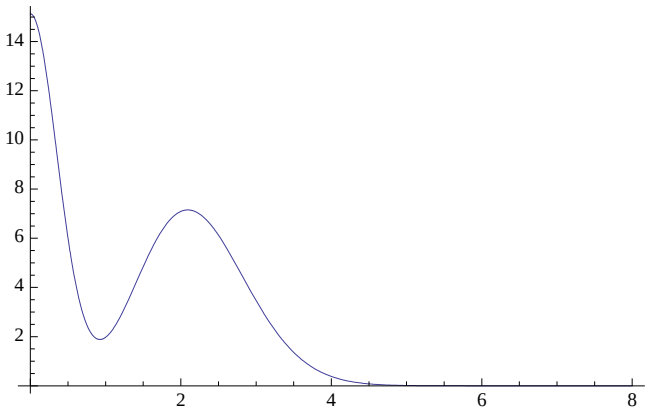


FIGURE 15. *Case $R = 7$, $a = 1$ and $\lambda \approx 3.23$. One has to test if the solution to the ODE system with same ansatz as in Fig. 14 is in the space $H^1(0,\infty;n_a\,r\,dr)$. The plot of $r \mapsto (|f'|^2 + [f|^2)\,n_a$ is shown above. Clearly the solution found numerically is admissible.*

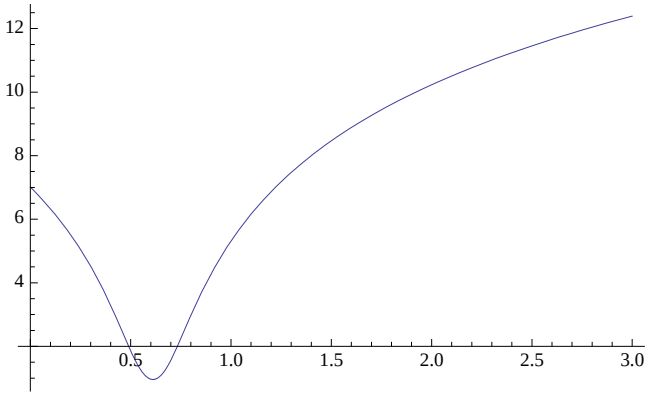


FIGURE 16. *Plot of $p \mapsto \log(1 + h(a,\lambda,p,R)^2)$ for $a = 1$, $\lambda = 0.5$. The difficulty comes from the instability of the solutions with respect to the parameters $\lambda$ and $p$. If the function $f$ is not in the space $H^1(0,\infty;n_a\,r\,dr)$, then $h(a,\lambda,p,R)^2$ uniformly diverges as $R \to +\infty$. A possible method is therefore to find the value of $p$ that realizes the minimal value of $h(a,\lambda,p,R)^2$ for a given $R > 0$, and then select for which value of $\lambda$ this quantity converges to a finite value as $R \to +\infty$. In practice, only rather small values of $R$ can be taken into account, which makes the method inaccurate. Here $R = 3$.*

The main advantage in the approach used for plotting Fig. 14 is that the expression of $\psi'(0)$ was explicitly known in terms of $a$, at least for one

solution. This, however, suggests a new shooting criterion, which goes as follows.

Solutions corresponding to $k = 1$ have to solve the Poisson equation

$$-\Delta\left(\psi(r)\,\frac{x_1}{r}\right) = n_a(r)\,f(r)\,\frac{x_1}{r}\,, \quad r = |x|\,, \quad x = (x_1, x_2) \in \mathbb{R}^2$$

with $i = 1$, 2, and can be expressed as

$$\Psi(x) := \psi(r)\,\frac{x_1}{r} = -\frac{1}{2\pi}\int_{\mathbb{R}^2} \log|x-y| * n_a(|y|)\,f(|y|)\,\frac{y_1}{|y|}\,dx\,.$$

Consider the case $i = 1$ and let $\theta \in [0, 2\pi)$ be such that $\frac{x_1}{r} = \cos\theta$.

$$(1,0)\cdot\nabla\Psi(0) = \psi'(0) = -\frac{1}{2\pi}\int_0^{2\pi}\cos^2\theta\,d\theta\int_0^\infty n_a(r)\,f(r)\,dr$$
$$= -\frac{1}{2}\int_0^\infty n_a(r)\,f(r)\,dr\,.$$

Notice that

$$\int_0^\infty n_a(r)\,f(r)\,dr = \int_{\mathbb{R}^2}\frac{n_a(|x|)\,f(|x|)}{2\pi\,|x|}\,dx\,.$$

This observation provides a new shooting criterion (see Figs. 17 and 18): any solution has to satisfy the condition

$$s(a,\lambda,p) = 0 \quad \text{where} \quad s(a,\lambda,p) := \left(2\,p + \int_0^\infty n_a(r)\,f(r)\,dr\right)^2\,,$$

where $f$ and $\psi$ are solutions with $f(0) = 0$, $f'(0) = 1$, $\psi(0) = 0$ and $p = -\psi'(0)$. Notice that we recover that $\psi'(0) = \frac{1}{2}\,e^a$ if $f(r) = \phi'(r) - r$, with $f(0) = 0$ and $f'(0) = \phi''(0) - 1 = -(1 + \frac{1}{2}\,e^a)$, or, if we impose $f'(0) = 1$ (which can always be done because we solve a linear problem), $\psi'(0) = -\frac{e^a}{e^a+2}$.

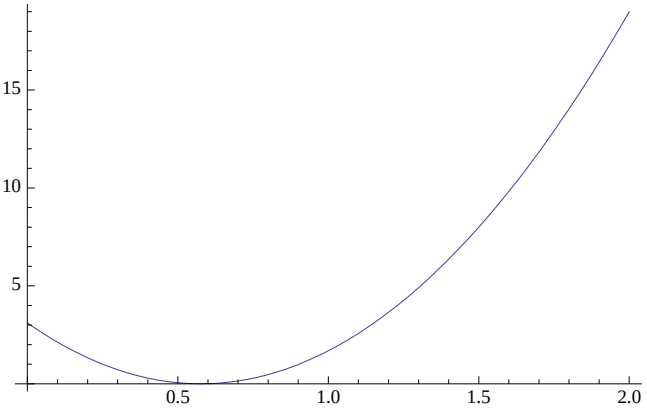


FIGURE 17. *Plot of $p \mapsto s(a,\lambda,p)$ for $a = 1$ and $\lambda = 1$. We numerically recover the fact that $p = \frac{e^a}{e^a+2} \approx 0.576117$.*

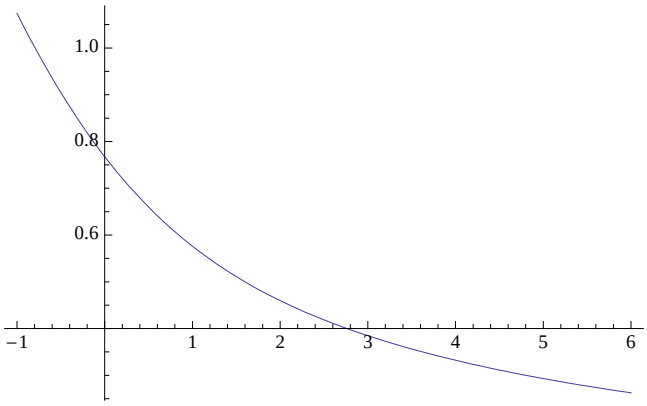


FIGURE 18. *Solving* $s(a,\lambda,p)=0$ *determines* $p=p(a,\lambda)$. *Here is shown the plot of* $\lambda\mapsto p(a,\lambda)$ *for* $a=1$.

By considering a shooting criterion similar to the one for $k=0$, we obtain the spectrum of $-\mathcal{L}_a^{(1)}$. See Fig. 19. This completes the study of the spectrum corresponding to $k=1$. Plotting the spectrum of $-\mathcal{L}_a^{(1)}$ as a function of $a$, or equivalently as a function of the mass $M$ can now be done: see Figs. 19 and 20.

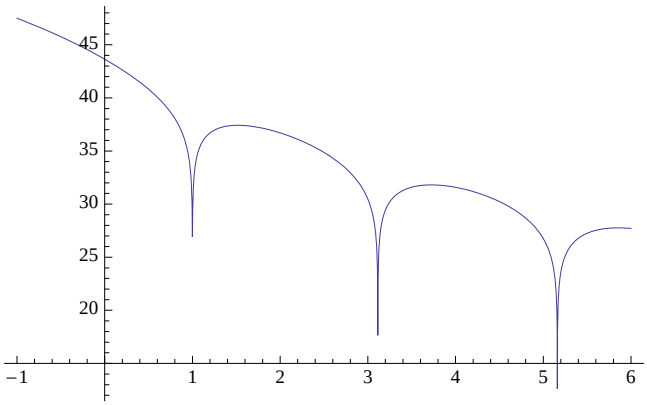


FIGURE 19. *Plot of* $\lambda\mapsto\log\left(1+f(\lambda,R)^2\right)$ *with* $R=7$, $a=1$, *where* $r\mapsto f(\lambda,r)$ *is the solution to*

$$\mathcal{L}_a^{(1)}f+\lambda\,f=0$$

*such that* $f(0)=1$ *and* $f'(0)=0$, $\psi(0)=0$ *and* $\psi'(0)=-p(a,\lambda)$. *In the limit* $R\to\infty$, *the first minimum (from the left) is located exactly at* $\lambda=1$. *Each minimum determines an eigenvalue of* $-\mathcal{L}_a^{(1)}$.

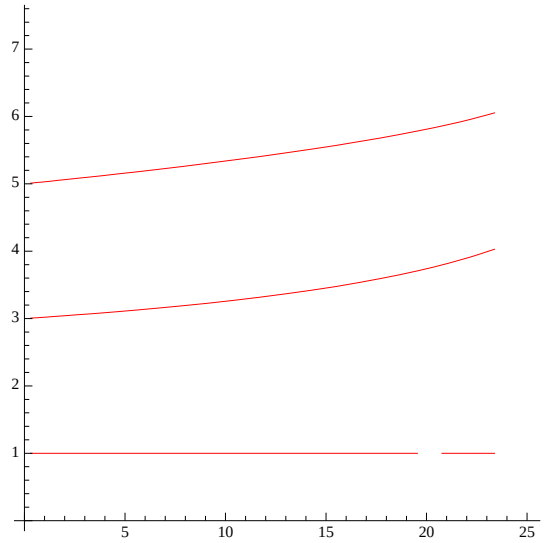


FIGURE 20. *Lowest eigenvalues of* $-\mathcal{L}_a^{(1)}$ *as a function of* $M(a)$. *Missing values corresponding to* $\lambda = 1$ *are due to numerical errors.*

Wit these results in hands, it is easy to check that $\lambda_{1,0} = 1$ for any $M \in (0, 8\pi)$. As a consequence, the spectral gap of $-\mathcal{L}_a$ is $\lambda_{1,0} - \lambda_{0,0} = 1$. See Fig. 21.

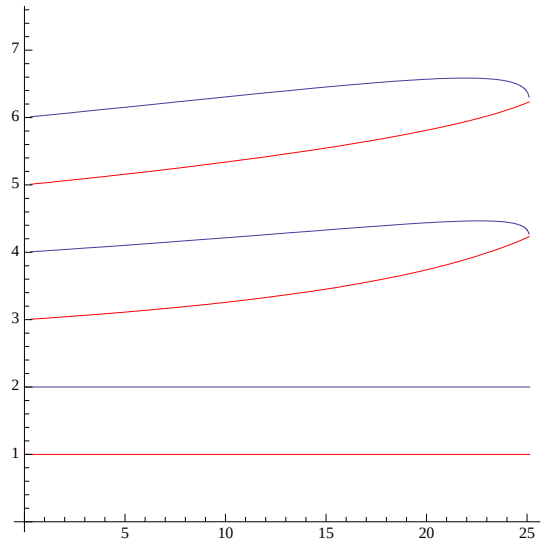


FIGURE 21. *Results of Figs. 11 and 20 are shown on a single picture. The lowest eigenvalues of* $-\mathcal{L}_a$ *are therefore* 0, 1 *and* 2, *thus establishing that the spectral gap of* $-\mathcal{L}_a$ *is* 1.

For higher values of $k$, that is $k \geq 2$, the same numerical methods than for $k = 1$ holds. Numerically we observe (see Fig. 22) that the lowest eigenvalue for $k = 2$ is $\lambda_{2,0}$ which takes values larger than 4. The branch originates from $\lambda = 4$ when $M \to 0_+$.

As a consequence, the lowest eigenvalues of $\mathcal{L}$ are

$$\lambda_{0,0} = 0 < \lambda_{1,0} = 1 < \lambda_{0,1} = 2 < 3 < \lambda_{1,1} < \lambda_{0,2} < \lambda_{2,0}$$

but $\lambda_{1,1}$ is not constant as $M$ varies in $(0, 8\pi)$.

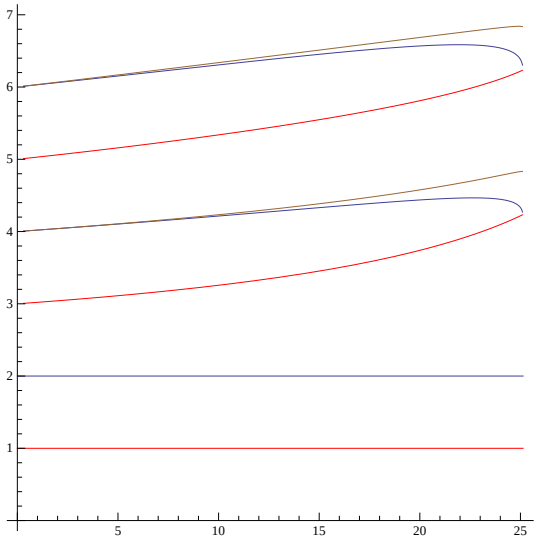


FIGURE 22. *Lowest eigenvalues, for $k = 0$ (blue), $k = 1$ (red) and $k = 2$ (brown).*

## 4. Concluding remarks

From a physics viewpoint, understanding why 0, 1 and 2 are eigenvalues is not very difficult.

(1) The stationary solution depends on the mass. Differentiating the equation with respect to the mass parameter immediately provides an element of the kernel, which turns out to be one-dimensional as can be shown by elementary considerations (uniqueness of the solution to an ODE by the Cauchy-Lipschitz theorem). As far as we are interested in the long time asymptotics of the solutions to (2), such a degree of freedom is not relevant for the evolution problem because the conservation of mass uniquely determines the limiting stationary solution.

(2) The Keller-Segel model before rescaling is an autonomous system: it does not depend explicitly on $x$. Any translation of the initial datum gives rise to a solution to the evolution problem translated by the same quantity, and it is straightforward to realize that the position

of the center of mass is preserved along the evolution. In the rescaled variables, it is clear that a solution corresponding to an initial datum made of a decentered self-similar profile exponentially converges towards the same self-similar profile, but centered. When linearizing, this provides an eigenmode (that can be computed by applying the operators which infinitesimally generate the translations, $\partial/\partial x_1$ or $\partial/\partial x_2$) and a direct computation shows that the corresponding eigenvalue is 1.

(3) The reason why $x \cdot \nabla$ also generates an eigenmode is slightly more subtle. In the original variables, the self-similar solutions explicitly depend on $t$, and a shift in $t$ amounts to a scaling of the self-similar solutions. Notice indeed that a solution translated in $t$ is still a solution. Once the self-similar change of variables has been done, any shift with respect to $t$ amounts to a scaling on the solution and thus explains why 2 is an eigenvalue.

More details on mathematical aspects of these observations can be found in [6]. Hence it is easy to understand why 0, 1 and 2 are eigenvalues, independently of the mass $M$. We have moreover identified the invariances that explain such facts. In the limit $M \to 0_+$, it has been observed in [3] that the spectrum of $\mathcal{L}$ is the same as the Fokker-Planck operator.

It has been stablished in [6] that the spectrum of $\mathcal{L}$ governs the rate of convergence of the solutions to (2): *for any $M \in (0, 8\,\pi)$, if $n_0 \in L^2_+(n^{-1}\,dx)$ and $M := \int_{\mathbb{R}^2} n_0\,dx < 8\,\pi$, then any solution to (2) with initial datum $n_0$ satisfies*

$$\int_{\mathbb{R}^2} |n(t,x) - n_\infty(x)|^2\,\frac{dx}{n_\infty(x)} \le C\,e^{-2\,\lambda\,t} \quad \forall\, t \ge 0$$

*for some positive constant $C$, where $n_\infty$ is the unique stationary solution to (2) with mass $M$ and*

$$\lambda = \lambda_{1,0} = 1\ ,$$

*provided the following technical condition is satisfied*

$$\exists\, \varepsilon \in (0, 8\,\pi - M) \quad \text{such that} \quad \int_0^s u_{0,*}(\sigma)\,d\sigma \le \int_{B\left(0,\sqrt{s/\pi}\right)} n_{\infty,M+\varepsilon}(x)\,dx$$

*for any $s \ge 0$. Here $u_{0,*}(\sigma)$ stands for the symmetrized function associated to $n_0$.*

If additionally the initial datum satisfies $\int_{\mathbb{R}^2} x\,n_0\,dx = 0$, then

$$\lambda = \lambda_{0,1} = 2\ .$$

Based on a similar approach that has been developed in the framework of the fast diffusion equation in [8], we can even define the *best matching asymptotic profile* as the function $\tilde{n}_\infty(t,x) = n_{\infty,\sigma(t)}(x)$ where $n_{\infty,\sigma} := \sigma^2\,n_\infty(\sigma\cdot)$ and $\sigma = \sigma(t)$ realizes the infimum

$$\mu \mapsto \int_{\mathbb{R}^2} |n(t,x) - n_{\infty,\mu}(x)|^2\,\frac{dx}{n_{\infty,\mu}(x)}\ .$$

If $\int_{\mathbb{R}^2} x\, n_0\, dx = 0$, then it follows from an analysis similar to the one of [8] that

$$\int_{\mathbb{R}^2} |n(t,x) - \tilde{n}_\infty(x)|^2 \, \frac{dx}{\tilde{n}_\infty(x)} \le C\, e^{-2\,\lambda_{1,1}\,t} \quad \forall\, t \ge 0$$

and our numerical results show that $\lambda_{1,1} \ge 3$.

## References


[1] P. Biler, *Growth and accretion of mass in an astrophysical model*, Appl. Math. (Warsaw), 23 (1995), pp. 179–189.

[2] P. Biler, G. Karch, P. Laurençot, and T. Nadzieja, *The $8\pi$-problem for radially symmetric solutions of a chemotaxis model in the plane*, Math. Methods Appl. Sci., 29 (2006), pp. 1563–1583.

[3] A. Blanchet, J. Dolbeault, M. Escobedo, and J. Fernández, *Asymptotic behaviour for small mass in the two-dimensional parabolic-elliptic Keller-Segel model*, Journal of Mathematical Analysis and Applications, 361 (2010), pp. 533 – 542.

[4] A. Blanchet, J. Dolbeault, and B. Perthame, *Two-dimensional Keller-Segel model: optimal critical mass and qualitative properties of the solutions*, Electron. J. Differential Equations, 44, 32 pages (2006).

[5] V. Calvez and J. A. Carrillo, *Refined asymptotics for the subcritical Keller-Segel system and related functional inequalities*. Preprint ArXiv 1007.2837, to appear in Proc. AMS, Article electronically published on February 23, 2012.

[6] J. Campos and J. Dolbeault, *Asymptotic estimates for the parabolic-elliptic Keller-Segel model in the plane*. Preprint, 2012.

[7] J. Dolbeault and B. Perthame, *Optimal critical mass in the two-dimensional Keller-Segel model in $\mathbb{R}^2$*, C. R. Math. Acad. Sci. Paris, 339 (2004), pp. 611–616.

[8] J. Dolbeault and G. Toscani, *Fast diffusion equations: matching large time asymptotics by relative entropy methods*, Kinetic and Related Models, 4 (2011), pp. 701–716.

[9] W. Jäger and S. Luckhaus, *On explosions of solutions to a system of partial differential equations modelling chemotaxis*, Trans. Amer. Math. Soc., 329 (1992), pp. 819–824.

[10] E. Keller and L. Segel, *Initiation of slime mold aggregation viewed as an instability*, Journal of Theoretical Biology, 26 (1970), pp. 399–415.

[11] T. Nagai, *Blow-up of radially symmetric solutions to a chemotaxis system*, Adv. Math. Sci. Appl., 5 (1995), pp. 581–601.

[12] Y. Naito and T. Suzuki, *Self-similar solutions to a nonlinear parabolic-elliptic system*, in Proceedings of Third East Asia Partial Differential Equation Conference, vol. 8, 2004, pp. 43–55.

[13] C. S. Patlak, *Random walk with persistence and external bias*, Bull. Math. Biophys., 15 (1953), pp. 311–338.

[14] B. Perthame, *Transport equations in biology*, Frontiers in Mathematics, Birkhäuser Verlag, Basel, 2007.


*Acknowledgments.* The authors acknowledge support by the ANR projects *CBDif-Fr* and *EVOL* (JD), and by the MathAmSud project *NAPDE* (JC and JD).

J. Dolbeault, J. Campos: Ceremade UMR CNRS nr. 7534, Université Paris Dauphine, Place de Lattre de Tassigny, 75775 Paris Cedex 16, France

J. Campos: Departamento de Ingeniería Matemática and CMM, Universidad de Chile, Casilla 170 Correo 3, Santiago, Chile